

Are shocks in conserved driven single-file motions with bottlenecks universal?

Sourav Pal^{1,*} and Abhik Basu^{1,†}

¹*Theory Division, Saha Institute of Nuclear Physics, a CI of Homi Bhabha National Institute, 1/AF Bidhannagar, Calcutta 700064, West Bengal, India*

Driven single-file motion sets the paradigm for wide variety of one-dimensional directed movements, ranging from intracellular transport and urban traffic to ant trails and controlled robot swarms. Motivated by the phenomenologies of these systems in closed geometries, regulated by number conservation and bottlenecks, we explore the domain walls (DWs) or shocks in a conceptual one-dimensional cellular automaton with a fixed particle number and a bottleneck. For high entry and exit rates of the cellular automaton, and with sufficiently large particle numbers, the DWs formed are independent of the associated rate parameters, revealing a *hitherto unknown universality* in their *shapes*. In contrast, the DWs do depend upon these parameters, if they are small, and hence have nonuniversal shapes. Our predictions on the DWs are testable in experiments.

Driven single-file motion (DSFM) is the cornerstone of effective one-dimensional (1D) transport in physical systems of diverse origin. This includes intracellular transport, e.g., motion of molecular motors along eukaryotic cells [1], ribosome translocation along messenger RNA (mRNA) strands [2–4], vehicular or pedestrian traffic along closed network of roads [5–7], ecological examples like ant trails [8, 9] and also 1D motion of robot swarms [10]. A key question is the nature of the stationary densities and their dependence on the underlying control parameters. In closed systems of DSFM connected to a particle storage or reservoir, regulated by the interplay of the overall fixed availability of particles, DSFM-reservoir couplings and bottlenecks, the stationary density profiles and their degree of *universality* vis-à-vis the control parameters in the system remains a theoretically and phenomenologically paramount issue.

In this Letter, motivated by the above generic issues in DSFM, we propose and study a conceptual 1D cellular automaton having a fixed number of available particles with only excluded volume interactions, and a bottleneck, based on totally asymmetric simple exclusion process (TASEP) [11–13]. We use it to explore universal shapes of the domain wall (DW) in the nonequilibrium steady states of the model.

Originally proposed to study protein synthesis in eukaryotic cells [14], TASEP has subsequently emerged as a paradigmatic 1D model for nonequilibrium phase transitions in open boundary [11–13, 15–17], and closed geometries [18–28]. More recently, considerations of the finite availability of ribosomes in the protein synthesis in cells [29] have led to studies of TASEP lanes connected to particle reservoirs, revealing the role of global particle number conservation (PNC) [30–41].

Our model consists of a TASEP on a 1D lattice with L sites ($j = 1, 2, \dots, L$), each having maximum occupancy 1, with unit hopping rate, except at the defect site at $j = L/2$, where hopping rate $q < 1$; see Fig. 1. Here, the

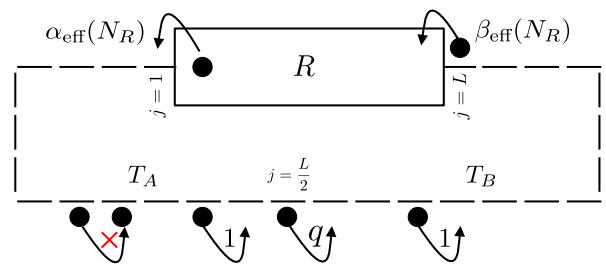


FIG. 1: **Schematic model diagram.** A 1D lattice executing TASEP with hopping rate $q < 1$ at a point defect and unity elsewhere is connected to a particle reservoir R at both ends. Effective entry and exit rates, α_{eff} and β_{eff} respectively, depend explicitly on reservoir population N_R . See text.

effective entry rate α_{eff} and exit rate β_{eff} are

$$\alpha_{\text{eff}}(N_R) = \alpha f(N_R), \quad (1)$$

$$\beta_{\text{eff}}(N_R) = \beta(1 - f(N_R)). \quad (2)$$

A monotonically rising function, $f(N_R)$, of reservoir population N_R describes the TASEP-reservoir couplings. It is physically reasonable to assume α_{eff} increasing with N_R while β_{eff} decreases [30, 38, 39]. For simplicity, we choose $f(N_R) = N_R/N^* \in [0, 1]$ [38–41], N^* is a normalization factor and $\alpha, \beta \geq 0$; see also Ref. [42]. We define $\mu \equiv N_0/L$, where $N_0 \equiv N_R + \sum_{j=1}^L n_j$ is the total particle number, a constant of motion, with $n_j = 0, 1$, the occupation number of site j . The stationary states are parametrized by α, β, μ, q, f . Parameters α, β control the mutual interplay between the “supply” and “demand” in finite-resources systems, and model the DSFM-reservoir couplings, e.g., in mRNA translation [43].

As specific examples, we consider (i) Case I: $N^* = L$ and (ii) Case II: $N^* = N_0$. Since $\beta_{\text{eff}} > 0$, and using PNC, we must have (i) $N_0 \leq 2L$ or $0 \leq \mu \leq 2$ for $N^* = L$, corresponding to a finite carrying capacity of the reservoir for a given size L of the TASEP lane; (ii) no such constraint on N_0 appears when $N^* = N_0$, allowing the model to accommodate any number of particles, i.e., $0 \leq \mu < \infty$, implying unrestricted carrying capacity

of the reservoir. See also Refs. [39, 40] in this context. Only for $N^* = L$ (but not for $N^* = N_0$), our model admits the particle-hole symmetry: $\alpha \leftrightarrow \beta$ and $\mu \leftrightarrow 2 - \mu$; see Supplemental Material (SM) [44] for details.

We show that generically for sufficiently large α , β , and μ , the defect in the TASEP lane can induce DWs that have *universal shapes*, independent of α , β , μ , and the form of f , *always* located at the midpoint of the TASEP lane, with their heights depending *solely* on q . Rather intriguingly, such a DW is necessarily associated with a pair of *nonuniversal* boundary layers (BLs) depending on model parameters at the two ends of the TASEP lane, in contrast to usual TASEPs with open boundaries [16] or with finite resources [30–32, 38–41]. Thus, measurement of such a DW tells us *nothing* about α , β , μ , f , and is reminiscent of universal critical phenomena [45]. Identification of this DW phase, dubbed the universal DW (UDW) phase, which replaces the maximal current (MC) phase, and the role of *two* BLs in UDW formation are the principal results in this Letter. For other choices of α , β , conventional DWs without BLs emerge, induced by either by the defect or reservoir. Lastly, a pair of *nonuniversal delocalized domain walls* (DDWs) appear for α , β on a curve in the α - β plane, determined by the *competition* between the reservoir and defect.

For very low values of μ , the bulk of the TASEP lane remains in the low-density (LD) phase. As μ rises, it moves to DW phases, controlled either by the defect or the reservoir, eventually reaching the high-density (HD) phase at large μ ; see movies 1 and 2 in SM [44]. See the phase diagrams in Fig. 2 in the α - β plane for various μ -values with $q = 0.1$, for both $N^* = L$, N_0 , which differ significantly from that of an open TASEP [16].

Partly related models and studies appear in Ref. [46], which investigates steady states with resource-dependent hopping rates and a slow site, and in Ref. [47], which focuses on DWs. With $N^* = N_0$ and $q = 1$, our model reduces to that studied in Ref. [38].

To calculate the phases and phase diagrams, we employ mean-field theory (MFT) [16] for the TASEP lane by modeling it as two segments, T_A and T_B , connected at the defect site $j = L/2$, each with their effective entry and exit rates. The MFT results are validated through extensive Monte Carlo simulations (MCS). Introducing the quasi-continuous coordinate $x \equiv j/L$ in the thermodynamic limit (TL), $L \rightarrow \infty$, with $0 \leq x \leq 1$, we define the local density in segment T_m by $\rho_m(x) \equiv \langle \rho_j^m \rangle$, where ρ_j^m is the occupation at site j , $m = A, B$ and $\langle \dots \rangle$ indicates temporal averaging in the steady state.

With $(\alpha_{\text{eff}}, \beta_A)$ as the effective entry and exit rates for T_A , and $(\alpha_B, \beta_{\text{eff}})$ as those for T_B , stationary current conservation at $j = L/2$ and $j = (L/2) + 1$ gives

$$\beta_A = q(1 - \rho_{(L/2)+1}), \quad \alpha_B = q\rho_{L/2}. \quad (3)$$

Additionally, current through the defect site reads

$$J_d = q\rho_{L/2}(1 - \rho_{(L/2)+1}) = \alpha_B\beta_A/q. \quad (4)$$

Denoting the steady-state mean density and current respectively by ρ_m and J_m for segment T_m , $m = A, B$, current conservation $J_A = J_B = J_d$ implies either $\rho_A = \rho_B$ or $\rho_A + \rho_B = 1$. In analogy with an open TASEP, the bulk density in the LD-LD phase is given by $\rho_A = \alpha_{\text{eff}}(N_R) = \alpha f(N_R) = \rho_B = \alpha_B$ (from current conservation), controlled by the reservoir. Equation (3) together with PNC gives:

$$\rho_{\text{LD-LD}} = \begin{cases} \mu\alpha/(1 + \alpha), & N^* = L, \\ \mu\alpha/(\mu + \alpha), & N^* = N_0, \end{cases} \quad (5)$$

vanishing, unsurprisingly, for $\mu \rightarrow 0$. The defect imposes only a local jump of height $h = \alpha_{\text{eff}}(1 - q)/q > 0$ with a vanishing thickness in the TL behind it, as obtained by using current conservation in the steady-state [20].

The point defect can impose a DW behind it for larger μ , connecting LD and HD segments with densities ρ_{LD} and ρ_{HD} respectively. Stationary current conservation across the point defect gives [18, 23]

$$\rho_{\text{LD}} = q/(1 + q) = 1 - \rho_{\text{HD}}. \quad (6)$$

With $q \neq 1$, $\rho_{\text{HD}} > \rho_{\text{LD}}$. Thus, *if* the defect controls the steady-state, there cannot be any MC phase.

Qualitatively, as N_0 (or μ) increases, $\rho_{\text{LD-LD}}$ rises [Eq. (5)], eventually reaching the defect-limited value $\rho_{\text{LD-LD}} \equiv \alpha_{\text{eff}} = q/(1 + q)$. A DW is formed in T_A at $x = 1/2$, marking the onset of the DW-LD phase. With $\Theta(x) = 1$ (0) for $x >$ ($<$) 0 , for a DW in T_A , $\rho_A(x) = \rho_{\text{LD}} + \Theta(x - x_{w_1})(\rho_{\text{HD}} - \rho_{\text{LD}})$, where ρ_{LD} and ρ_{HD} are as given in (6), and x_{w_1} is the DW position. PNC gives

$$x_{w_1} = \begin{cases} [(1/2 - \mu)(1 + q) + q/\alpha]/(1 - q), \\ [(1/2 - \mu)(1 + q) + \mu q/\alpha]/(1 - q). \end{cases} \quad (7)$$

for $N^* = L$ (top) and $N^* = N_0$ (bottom). Substituting $x_{w_1} = 1/2$ in Eq. (7) gives the boundary between LD-LD and DW-LD phases: $\mu\alpha/(1 + \alpha) = q/(1 + q)$ for $N^* = L$, and $\mu\alpha/(\mu + \alpha) = q/(1 + q)$ for $N^* = N_0$ [see Figs. 2(a)-2(e)]. As μ or α increases (with other parameters fixed), more particles enter the TASEP lane, pushing the DW leftwards, keeping α_{eff} unchanged, until $x_{w_1} = 0$ at the onset of UDW phase. With $x_{w_1} = 0$ in Eq. (7), $\alpha(\mu - 1/2) = q/(1 + q)$ for $N^* = L$, and $\alpha(1 - 1/2\mu) = q/(1 + q)$ for $N^* = N_0$ [see Figs. 2(b, c, e)] are the boundary between DW-LD and UDW phases, which do not depend on β .

For a DW at $x = 1/2$ with HD and LD segments covering T_A and T_B , respectively, BLs of vanishing thickness in TL form at $j = 1$ and $j = L$. Current conservation gives

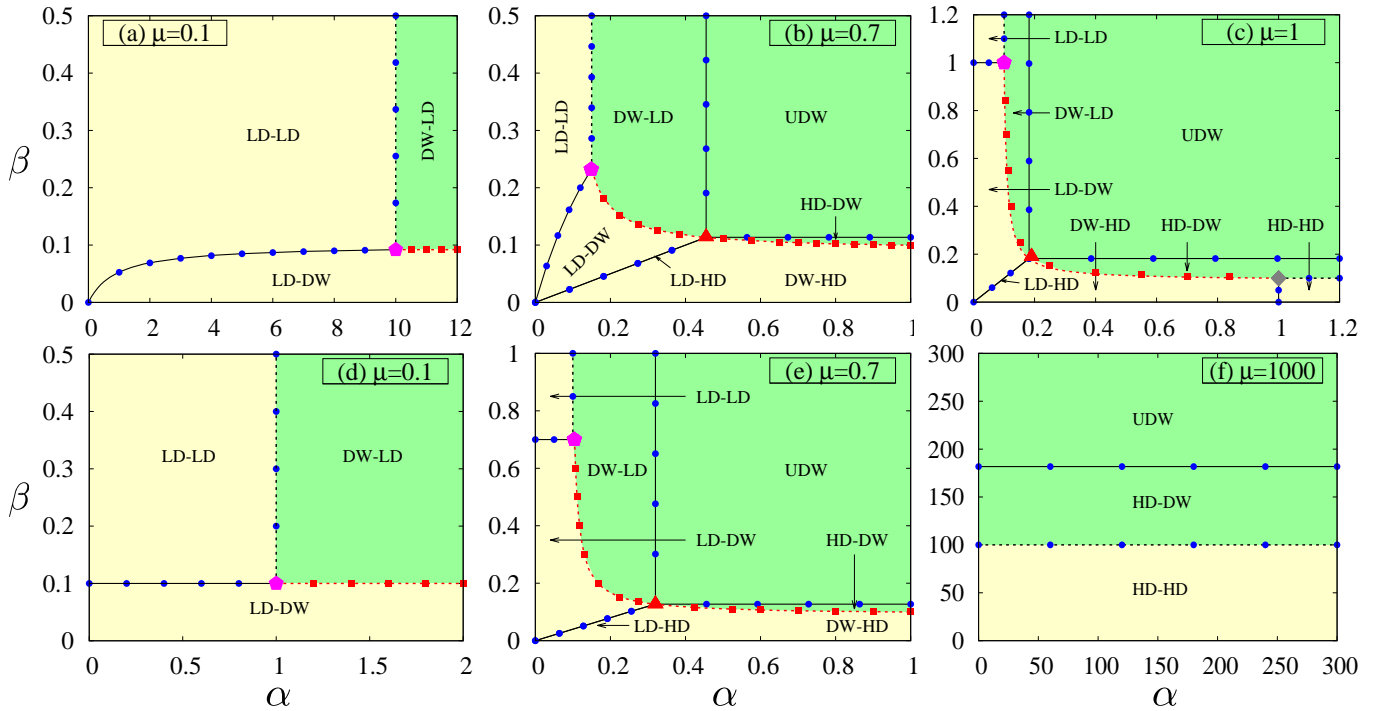


FIG. 2: Phase diagrams in the α - β plane at $q = 0.1$ for a set of representative values of μ : $N^* = L$ [upper panel (a-c)] and $N^* = N_0$ [lower panel (d-f)]. Reservoir- (defect-)controlled regions are shown in yellow (green). The different phases are marked. DDWs in both T_A and T_B are found along the red dashed curve (15) [subfigures (a-e)], which terminates at points marked \blacklozenge (magenta pentagon) and \blacklozenge (gray diamond), (see Table I in [44] for their coordinates), with complete delocalization occurring at point $(\tilde{\alpha}, \tilde{\beta})$ [see Eq. (16)] marked by a red triangle, and only partial elsewhere. Localized DWs appear in the remaining DW regions. MFT predictions (solid and dashed curves) agree well with MCS results (colored symbols). See text.

the α , β , f , μ , q -dependent *nonuniversal* BL densities

$$\rho_1 = [1 + q/\{(1+q)\alpha(\mu - 1/2)\}]^{-1}, \quad (8)$$

$$\rho_L = [1 + \{(1+q)\beta(3/2 - \mu)\}/q]^{-1} \quad (9)$$

for $N^* = L$; see SM [44] for $N^* = N_0$. As α and β increase with μ and q fixed, $\rho_1 \rightarrow 1$ and $\rho_L \rightarrow 0$, while the DW remains fixed at $x = 1/2$, defining the UDW phase. For larger μ , the DW however can move to T_B crossing the entry-end $x = 0$ of T_A (same as the exit-end $x = 1$ of T_B ; see Fig. 1), giving the HD-DW phase, and finally returns to $x = 1/2$ giving the HD-HD phase. Current conservation in UDW and HD-DW phases gives $\rho_{LD} = q/(1+q) = 1 - \rho_{HD}$. As $q \rightarrow 1$, the DW height, $\rho_{HD} - \rho_{LD}$, gradually decreases vanishing at $q = 1$, resulting in the MC phase. The UDW position is independent of *all* of α , β , q , μ , f , and the height depends *only* on q . Thus a UDW is controlled only by q . Hence in a renormalization group language, q appears as the only relevant operator in UDW phase, with everything else *irrelevant*, reminiscent of universal critical phenomena [45]; see also Ref. [26] for universality in disordered TASEP. PNC gives the DW position in HD-DW phase:

$$x_{w_2} = \begin{cases} [5/2 - \mu(1+q) + q(1/2 - 1/\beta)]/(1-q), \\ (3/2 - \mu q/\beta - q/2)/(1-q), \end{cases} \quad (10)$$

for $N^* = L$ (top) and $N^* = N_0$ (bottom). Substituting $x_{w_2} = 1$ in Eq. (10) gives the boundary between UDW and HD-DW phases: $\beta(3/2 - \mu) = q/(1+q)$ for $N^* = L$, and $\beta = 2\mu q/(1+q)$ for $N^* = N_0$ [see Figs. 2(b, c, e, f)], which are independent of α . Analogous to an open TASEP, the bulk density in the HD-HD phase is $\rho_A = 1 - \beta_A = \rho_B = 1 - \beta_{\text{eff}}(N_R)$ (current conservation). We get using Eq. (3) and PNC:

$$\rho_{\text{HD-HD}} = \begin{cases} (1 - \beta + \mu\beta)/(1 + \beta), & N^* = L, \\ \mu/(\mu + \beta), & N^* = N_0, \end{cases} \quad (11)$$

independent of q . Furthermore, the boundary between HD-HD and HD-DW phases is obtained from $x_{w_2} = 1/2$ in Eq. (10), giving $(2 - \mu)\beta/(1 + \beta) = q/(1 + q)$ for $N^* = L$, and $\beta = \mu q$ for $N^* = N_0$ [see Figs. 2(c, f)].

There is another mechanism for DW formation. Depending on the parameters, upon raising μ starting from the LD-LD phase, before hitting the threshold $\alpha_{\text{eff}} = q/(1+q)$, it can reach another threshold satisfying $\alpha_{\text{eff}} = \beta_{\text{eff}}$, for which a DW is formed at $x = 1$, beginning the LD-DW phase. Further increase in μ pushes the DW towards $x = 0$, going through the LD-DW, LD-HD (when the DW is at $x = 1/2$; see also below) and DW-HD phases – finally reaching the HD-HD phase. With $\alpha_{\text{eff}} = \beta_{\text{eff}}$ in the DW phase, we get $f(N_R) = \beta/(\alpha + \beta)$,

for both $N^* = L, N_0$, giving DW densities as

$$\rho_{LD} = \alpha\beta/(\alpha + \beta) = 1 - \rho_{HD}, \quad (12)$$

independent of q . By PNC, the DW location x_{w_3} is

$$x_{w_3} = \begin{cases} [\alpha + 2\beta - \mu(\alpha + \beta) - \alpha\beta]/(\alpha + \beta - 2\alpha\beta), \\ (\alpha + \beta - \mu\alpha - \alpha\beta)/(\alpha + \beta - 2\alpha\beta), \end{cases} \quad (13)$$

for $N^* = L$ (top) and $N^* = N_0$ (bottom). The DW shape, being controlled by α, β, μ , and f is clearly *nonuniversal*. Substituting $x_{w_3} = 1$ in Eq. (13) provides the boundary between LD-LD and LD-DW phases: $\mu/(1+\alpha) = \beta/(\alpha+\beta)$ for $N^* = L$ and $\beta = \mu$ for $N^* = N_0$ [see Figs. 2(a)-2(e)]. Next, $x_{w_3} = 1/2$ in Eq. (13) gives the boundary between LD-DW and LD-HD phases: $\beta/(\alpha+\beta) = \mu - 1/2$ for $N^* = L$ and $\beta/(\alpha+\beta) = 1 - 1/2\mu$ for $N^* = N_0$ [see Figs. 2(b, c, e)]. Lastly, the boundary between DW-HD and HD-HD phases is obtained from $x_{w_3} = 0$ in Eq. (13): $\alpha/(\alpha + \beta) = (2 - \mu)/(1 + \beta)$ for $N^* = L$ and $\alpha/(\alpha + \beta) = 1/(\mu + \beta)$ for $N^* = N_0$.

The LD-DW and DW-HD phases are separated by the LD-HD phase line $\mathcal{L}(\alpha, \beta, \mu) = 0$, obtained by setting $x_{w_3} = 1/2$ in Eq. (13) giving

$$\mathcal{L}(\alpha, \beta, \mu) = \begin{cases} [(\alpha + 3\beta)/2(\alpha + \beta)] - \mu, \\ [(\alpha + \beta)/2\alpha] - \mu, \end{cases} \quad (14)$$

for $N^* = L$ (top) and $N^* = N_0$ (bottom). Stationary densities for α, β on (14) is a *nonuniversal* DW at $x = 1/2$ but have a shape distinct from a UDW; see SM [44]. Nonuniversal DWs are free of BLs.

A minimum current principle [41] determines whether DWs are defect- or reservoir-induced: when the corresponding stationary currents $J_{\text{def}} = q/(1+q)^2 < (>) J_{\text{res}} = \alpha\beta/(\alpha + \beta) [1 - \alpha\beta/(\alpha + \beta)]$, DWs are controlled by the defect (reservoir). This gives the surface

$$\alpha\beta/(\alpha + \beta) = q/(1 + q) \quad (15)$$

that separates the two regimes. Depending on μ and q , the curve (15) has one or two endpoints marked \heartsuit and \blacklozenge in the α - β plane [Figs. 2(a)-2(e), see [44] for details]. This curve demarcates the boundary between the LD-DW and DW-LD phases, and also between DW-HD and HD-DW phases. Accordingly, DW-LD and HD-DW phases appear in the defect-controlled (green) region, while LD-DW and DW-HD lie in the reservoir-controlled (yellow) region in Fig. 2; see also the movies [44]. Note that $\mathcal{L}(\alpha, \beta, \mu)$ terminates at

$$(\tilde{\alpha}, \tilde{\beta}) = \begin{cases} 2q/(1+q)(1/(2\mu-1), 1/(3-2\mu)), \\ 2\mu q/(1+q)(1/(2\mu-1), 1), \end{cases} \quad (16)$$

for $N^* = L$ (top) and $N^* = N_0$ (bottom), where $(\tilde{\alpha}, \tilde{\beta})$ is the point where $\mathcal{L} = 0$ and curve (15) intersect. Intriguingly, when $J_{\text{def}} = J_{\text{res}}$, i.e., when the defect ‘‘competes’’

with the reservoir, a new kind of state, a *pair of DDWs*, emerges for μ satisfying the conditions for DW formation due to both the defect and reservoir. Following the logic of the DW formation caused by the defect or reservoir, we expect one DW, say at $x = x_w^{\text{def}}$, in T_A due to and behind the defect, and another DW at $x = x_w^{\text{res}}$ in T_B due to and behind the reservoir. PNC gives only a linear relation between x_w^{def} and x_w^{res} ; any pair of $(x_w^{\text{def}}, x_w^{\text{res}})$ satisfying PNC is a valid solution. The inherent stochasticity of the underlying microscopic dynamics ensures that all such pairs of $(x_w^{\text{def}}, x_w^{\text{res}})$ are visited over time, giving one DDW in each of T_A and T_B [23], see Figs. 3(c, f). At $(\tilde{\alpha}, \tilde{\beta})$, DDWs are fully delocalized across T_A and T_B [red triangular point in Figs. 2(b, c, e)]. Moving away from $(\tilde{\alpha}, \tilde{\beta})$ on the curve (15), their spans gradually decrease, vanishing at the endpoints. Geometric constructions of the DDW profiles [44] that depend on the parameters and f (hence nonuniversal) show good agreement with the MCS results; see Fig. 4. Phase transitions across (15) are characterized by a jump in ρ , indicating a discontinuous transition; ρ varies continuously across other phase boundaries.

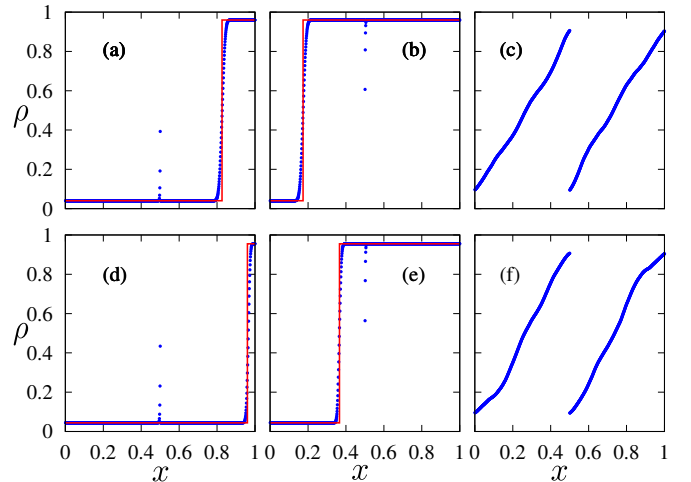


FIG. 3: LDWs in subplots (a, b, d, e) and DDWs in (c, f) for $q = 0.1$ ($L = 1000$). MFT (red solid lines) and MCS (blue circular points) results match well. Subplots (a, b, c): $N^* = L$ and subplots (d, e, f): $N^* = N_0$. (a) $\alpha = 0.05, \beta = 0.2, \mu = 1$; (b) $\alpha = 0.2, \beta = 0.05, \mu = 1$; (c) $\alpha = \beta = 0.19, \mu = 1$; (d) $\alpha = 0.05, \beta = 0.4, \mu = 0.7$; (e) $\alpha = 0.4, \beta = 0.05, \mu = 0.7$; and (f) $\alpha = 0.333, \beta = 0.1332, \mu = 0.7$.

In summary, we have shown that a DW in the present model can have universal shape, being independent of all parameters except q or nonuniversal, being controlled by several parameters. While we have shown these for two specific distinct choices of f , one with particle-hole symmetry and the other without, similar UDWs together with BLs should appear for any f with monotonic dependence on the reservoir population, although phase diagrams should depend nonuniversally on f . Our basic predictions can be observed in variety of situations, e.g.,

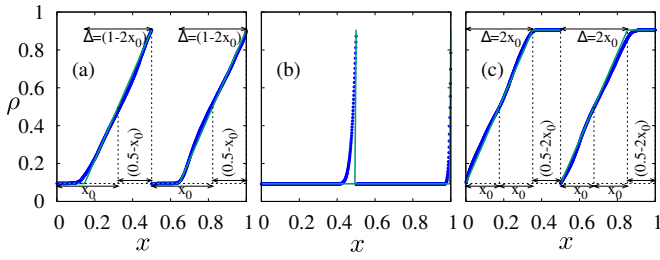


FIG. 4: Partial DDWs for parameters on the curve (15) away from $(\tilde{\alpha}, \tilde{\beta})$ for $N^* = L$. (a) $\alpha = 0.154, \beta = 0.25$; (b) $\alpha = 0.103, \beta = 0.95$; and (c) $\alpha = 0.25, \beta = 0.154$ with fixed $\mu = 1, q = 0.1$ for all. MCS results (blue circles) match very well with geometrical constructions of the DDW profiles (green solid lines), see [44] for the position and span of DDWs.

ribosome density profiling experiments [48, 49] on mRNA loops with rare “slow codon” or “pause sites” (which have distinct biological functions [50–52]) in biological cells, or simple video imaging of vehicles in closed urban roads with roadblocks and ant trails with local hindrance [53] and robot swarms [10]. Intriguingly, experimental detection of UDWs cannot reveal the model parameters and functions f , unless BLs are also resolved. Coarse-grained density measurement experiments do not suffice for that.

Experimental verification of these phenomena can be conveniently realized in model systems with inertial active particles, such as mm- to cm-sized robots, or external field-driven spherical structures in a narrow channel where the particles cannot cross each other. While the obstruction can be created using a spatially varying driving field, the controlled entry to (exit from) the channel from (to) the particle reservoir would require gating controlled by reservoir population. The latter and the channel population can be determined by live video imaging.

Our model can be made more realistic by introducing inter-particle interactions and allowing time-delays in the gates of the reservoir. From a theoretical perspective, it will be interesting to study the role of fluctuations in the DW phases by systematically going beyond MFT [54, 55].

Acknowledgement:- The authors thank M. Khan for helpful suggestions. A.B. thanks Alexander von Humboldt Stiftung (Germany) for partial financial support through their research group linkage programme (2024).

* Electronic address: isourav81@gmail.com

† Electronic address: abhik.123@gmail.com, abhik.basu@saha.ac.in

- [1] B. Alberts, *Molecular Biology of the Cell* (Garland, New York, 2008).
- [2] S. E. Wells, E. Hillner, R. D. Vale and A. B. Sachs, Circularization of mRNA by Eukaryotic Translation Initiation Factors, *Mol. Cell.* **2**, 135 (1998).
- [3] S. Wang, K. S. Browning and W. A. Miller, A viral se-

quence in the 3'-untranslated region mimics a 5' cap in facilitating translation of uncapped mRNA, *EMBO J.* **16**, 4107 (1997).

- [4] Y. Nakamura, T. Gojobori, and T. Ikemura, Codon usage tabulated from international DNA sequence databases: status for the year 2000, *Nucleic Acids Res.* **28**, 292 (2000).
- [5] D. Chowdhury, L. Santen and A. Schadschneider, Statistical physics of vehicular traffic and some related systems, *Phys. Rep.* **329**, 199 (2000).
- [6] D. Helbing, Traffic and related self-driven many-particle systems, *Rev. Mod. Phys.* **73**, 1067 (2001).
- [7] N. P. N. Ngoc, H. A. Thi, and N. V. Vinh, Exactly solvable dual bus-route model, *Phys. Rev. E* **110**, 054130 (2024).
- [8] D. Chowdhury, V. Guttal, K. Nishinari and A. Schadschneider, A cellular-automata model of flow in ant-trails: non-monotonic variation of speed with density, arXiv:cond-mat/0201207v3, *J. Phys.A* **35**, L573 (2002).
- [9] N. P. N. Ngoc, H. A. Thi, and N. V. Vinh, An exactly solvable model for single-lane unidirectional ant traffic, *Physica A: Statistical Mechanics and its Applications* **651**, 130022 (2024).
- [10] L. Alonso-Llanes, A. Garcimartín, and I. Zuriguel, *Phys. Rev. Research* **6**, L022037 (2024).
- [11] J. Krug, Boundary-induced phase transitions in driven diffusive systems, *Phys. Rev. Lett.* **67**, 1882 (1991).
- [12] B. Derrida, S. A. Janowsky, J. L. Lebowitz, and E. R. Speer, Exact solution of the totally asymmetric simple exclusion process: Shock profiles, *J. Stat. Phys.* **73**, 813 (1993).
- [13] B. Derrida and M. R. Evans, “Exact correlation functions in an asymmetric exclusion model with open boundaries”, *Journal de Physique I* **3**, 311 (1993).
- [14] C. T. MacDonald, J. H. Gibbs, and A. C. Pipkin, Kinetics of biopolymerization on nucleic acid templates, *Biopolymers* **6**, 1 (1968).
- [15] B. Derrida, M. R. Evans, V. Hakim, and V. Pasquier, Exact solution of a 1d asymmetric exclusion model using a matrix formulation, *J. Phys. A: Math. and Gen.* **26**, 1493–1517 (1993).
- [16] R. A. Blythe and M. R. Evans, Nonequilibrium steady states of matrix-product form: a solver’s guide, *J. Phys. A* **40**, R333 (2007).
- [17] T. Chou, K. Mallick, and R. K. P. Zia, Non-equilibrium statistical mechanics: from a paradigmatic model to biological transport, *Rep. Prog. Phys.* **74**, 116601 (2011).
- [18] S. A. Janowsky and J. L. Lebowitz, Finite-size effects and shock fluctuations in the asymmetric simple-exclusion process, *Phys. Rev. A* **45**, 618 (1992).
- [19] G. Tripathy and M. Barma, Driven lattice gases with quenched disorder: Exact results and different macroscopic regimes, *Phys. Rev. E* **58**, 1911 (1998).
- [20] P. Pierobon, M. Mabilia, R. Kouyos, and E. Frey, Bottleneck-induced transitions in a minimal model for intracellular transport, *Phys. Rev. E* **74**, 031906 (2006).
- [21] H. Hinsch and E. Frey, Bulk-driven nonequilibrium phase transitions in a mesoscopic ring, *Phys. Rev. Lett.* **97**, 095701 (2006).
- [22] R. Chatterjee, A. K. Chandra, and A. Basu, Phase transition and phase coexistence in coupled rings with driven exclusion processes, *Phys. Rev. E* **87**, 032157 (2013)
- [23] N. Sarkar and A. Basu, Nonequilibrium steady states in asymmetric exclusion processes on a ring with bottle-

- necks, *Phys. Rev. E* **90**, 022109 (2014).
- [24] T. Banerjee, N. Sarkar and A. Basu, Generic nonequilibrium steady states in an exclusion process on an inhomogeneous ring, *J. Stat. Mech. J. Stat. Mech.* P01024 (2015).
- [25] R. Chatterjee, A. K. Chandra, and A. Basu, Asymmetric exclusion processes on a closed network with bottlenecks, *J. Stat. Mech.* (2015) P01012
- [26] T. Banerjee and A. Basu, Smooth or shock: Universality in closed inhomogeneous driven single file motions, *Phys. Rev. Research* **2**, 013025 (2020).
- [27] P. Roy, A.K. Chandra, and A. Basu, Pinned or moving: states of a single shock in a ring, *Phys. Rev. E* **102**, 012105 (2020).
- [28] A. Goswami, R. Chatterjee, and S. Mukherjee, Defect versus defect: stationary states of single file marching in periodic landscapes with road blocks, arXiv: 2402.08499
- [29] B. Alberts, A. Johnson, P. Walter, and J. Lewis, *Molecular Biology of the Cell*, 5th ed. (Garland Publishing Inc., New York, 2008).
- [30] D. A. Adams, B. Schmittmann, and R. K. P. Zia, Far from equilibrium transport with constrained resources, *J. Stat. Mech.* (2008) P06009.
- [31] L. Jonathan Cook and R. K. P. Zia, Feedback and fluctuations in a totally asymmetric simple exclusion process with finite resources, *J. Stat. Mech.* (2009) P02012
- [32] L. J. Cook, R. K. P. Zia, and B. Schmittmann, Competition between multiple totally asymmetric simple exclusion processes for a finite pool of resources, *Phys. Rev. E* **80**, 031142 (2009).
- [33] R. Lipowsky, S. Klumpp, and T. M. Nieuwenhuizen, Random walks of cytoskeletal motors in open and closed compartments, *Phys. Rev. Lett.* **87**, 108101 (2001).
- [34] S. Klumpp and R. Lipowsky, Traffic of molecular motors through tube-like compartments, *J. Stat. Phys.* **113**, 233 (2003).
- [35] S. Klumpp and R. Lipowsky, Asymmetric simple exclusion processes with diffusive bottlenecks, *Phys. Rev. E* **70**, 066104 (2004).
- [36] L. D. Fernandes and L. Ciandrini, Driven transport on a flexible polymer with particle recycling: A model inspired by transcription and translation, *Phys. Rev. E* **99**, 052409 (2019).
- [37] O. Dauloudet, I. Neri, J.-C. Walter, J. Dorignac, F. Geniet, and A. Parmeggiani, Modelling the effect of ribosome mobility on the rate of protein synthesis, *Eur. Phys. J. E* **44**, 1 (2021).
- [38] A. Haldar, P. Roy, and A. Basu, Asymmetric exclusion processes with fixed resources: Reservoir crowding and steady states, *Phys. Rev. E* **104**, 034106 (2021).
- [39] S. Pal, P. Roy, and A. Basu, Availability, storage capacity, and diffusion: Stationary states of an asymmetric exclusion process connected to two reservoirs, *Phys. Rev. E* **110**, 054104 (2024).
- [40] S. Pal, P. Roy, and A. Basu, Distributed fixed resources exchanging particles: Phases of an asymmetric exclusion process connected to two reservoirs, *Phys. Rev. E* **111**, 034109 (2025).
- [41] A. Haldar, P. Roy, E. Frey, and A. Basu, Availability versus carrying capacity: Phases of asymmetric exclusion processes competing for finite pools of resources, *Phys. Rev. E* **111**, 014154 (2025).
- [42] T. Seppäläinen, Existence of hydrodynamics for the totally asymmetric simple K-exclusion process, *Ann. Probab.* **27**, 361 (1999).
- [43] C. A. Brackley, M.C. Romano and M. Thiel, The Dynamics of Supply and Demand in mRNA Translation, *PLoS Computational Biology* **7**, e1002203 (2011).
- [44] Supplemental Material containing details on the particle-hole symmetry for Case I, additional calculational details and movies.
- [45] P. M. Chaikin and T. C. Lubensky, *Principles of Condensed Matter Physics* (Cambridge University Press, Cambridge, 2000).
- [46] C. A. Brackley, M. C. Romano, and M. Thiel, Slow sites in an exclusion process with limited resources, *Phys. Rev. E* **82**, 051920 (2010).
- [47] L. J. Cook, J. J. Dong, and A. LaFleur, Interplay between finite resources and a local defect in an asymmetric simple exclusion process, *Phys. Rev. E* **88**, 042127 (2013).
- [48] N. T. Ingolia et al., Genome-Wide Analysis in Vivo of Translation with Nucleotide Resolution Using Ribosome Profiling, *Science* **324**, 218 (2009).
- [49] Y. Arava, F. Edward Boas, P. O. Brown and D. Herschlag, Dissecting eukaryotic translation and its control by ribosome density mapping, *Nucleic Acids Res.* **33**, 2421 (2005).
- [50] R. Brockmann, A. Beyer, J. J. Heinisch, and T. Wilhelm, Posttranscriptional Expression Regulation: What Determines Translation Rates?, *PLOS Comput. Biol.* **3**, e57 (2007).
- [51] I. J. Purvis, A. J. E. Bettany, T. C. Santiago, J. R. Coggins, K. Duncan, R. Eason, and A. J. P. Brown, The efficiency of folding of some proteins is increased by controlled rates of translation in vivo: A hypothesis, *J. Mol. Biol.* **193**, 413 (1987).
- [52] M. C. Romano, M. Thiel, I. Stansfield, and C. Grebogi, Queueing Phase Transition: Theory of Translation, *Phys. Rev. Lett.* **102**, 198104 (2009).
- [53] J. A. Sabattini, F. Sturniolo, M. Bollazzi, L. A. Bugnon, AntTracker: A low-cost and efficient computer vision approach to research leaf-cutter ants behavior, *Smart Agricultural Technology* **5**, 100252 (2023).
- [54] L. Bertini, A. D. Sole, D. Gabrielli, G. Jona-Lasinio and C. Landim, Macroscopic fluctuation theory, *Rev. Mod. Phys.* **87**, 593 (2015).
- [55] B. Doyon, G. Perfetto, T. Sasamoto, and T. Yoshimura, Ballistic macroscopic fluctuation theory, *SciPost Phys.* **15**, 136 (2023).

Supplemental Material for “Are shocks in conserved driven single-file motions with bottlenecks universal?”

EQUATIONS OF MOTION AND PARTICLE-HOLE SYMMETRY

In this section, we present the dynamical equations of motion (EOMs) for different sites of the TASEP lane and show that particle-hole symmetry is present in our model when $N^* = L$, but *not* when $N^* = N_0$. Let ρ_j denote the discrete particle density at site j . The EOMs are as follows:

$$\partial_t \rho_1 = \alpha_{\text{eff}}(1 - \rho_1) - \rho_1(1 - \rho_2), \quad (17)$$

$$\partial_t \rho_j = \rho_{j-1}(1 - \rho_j) - \rho_j(1 - \rho_{j+1}), \quad (18)$$

$$\partial_t \rho_L = \rho_{L-1}(1 - \rho_L) - \beta_{\text{eff}} \rho_L. \quad (19)$$

Equation (17) describes the entry site ($j = 1$), Eq. (18) applies to the bulk sites excluding $j = L/2$ and $j = (L/2) + 1$, i.e., for $1 < j < L/2$ and $(L/2) + 1 < j < L$, and Eq. (19) governs the exit site ($j = L$). For the central sites $j = L/2$ and $j = (L/2) + 1$, between which particles hop with reduced rate $q < 1$, the EOMs are:

$$\partial_t \rho_{\frac{L}{2}} = \rho_{\frac{L}{2}-1}(1 - \rho_{\frac{L}{2}}) - q\rho_{\frac{L}{2}}(1 - \rho_{\frac{L}{2}+1}), \quad (20)$$

$$\partial_t \rho_{\frac{L}{2}+1} = q\rho_{\frac{L}{2}}(1 - \rho_{\frac{L}{2}+1}) - \rho_{\frac{L}{2}+1}(1 - \rho_{\frac{L}{2}+2}). \quad (21)$$

We first consider Case I: $N^* = L$, for which the effective boundary rates are given by $\alpha_{\text{eff}} = \alpha f(N_R)$ and $\beta_{\text{eff}} = \beta(1 - f(N_R))$, with $f(N_R) = N_R/L$ and $0 \leq \mu \leq 2$. We aim to show that the EOMs (17)–(21) remain invariant under the following set of transformations:

$$\alpha \leftrightarrow \beta, \quad (22)$$

$$\rho_j \leftrightarrow 1 - \rho_{L-j+1}, \quad (23)$$

$$\mu \leftrightarrow 2 - \mu. \quad (24)$$

Let us first consider the entry-site EOM (17). Under transformation (23), we have $\rho_1 \leftrightarrow 1 - \rho_L$ and $\rho_2 \leftrightarrow 1 - \rho_{L-1}$. To examine how the function $f(N_R)$ transforms, we recall that $\mu = N_0/L$, and using the PNC relation $N_0 = N_R + \sum_{j=1}^L \rho_j$, we obtain:

$$f(N_R) = \frac{N_R}{L} = \mu - \frac{1}{L} \sum_{j=1}^L \rho_j. \quad (25)$$

Applying the transformations (23) and (24) to Eq. (25), we get:

$$\begin{aligned} f(N_R) &\leftrightarrow (2 - \mu) - \frac{1}{L} \left(L - \sum_{j=1}^L \rho_j \right) \\ &= 1 - \mu + \frac{1}{L} \sum_{j=1}^L \rho_j \\ &= 1 - f(N_R). \end{aligned} \quad (26)$$

Using transformations (22) and (26) together, we get

$$\alpha_{\text{eff}} = \alpha f(N_R) \leftrightarrow \beta(1 - f(N_R)) = \beta_{\text{eff}}. \quad (27)$$

Substituting all these transformed quantities into the entry-site EOM (17) maps it into the exit-site EOM (19). This demonstrates that particle injection at the left boundary is equivalent to hole extraction at the right boundary. A similar invariance holds for the bulk EOMs (18) corresponding to sites $1 < j < L/2$ and $(L/2) + 1 < j < L$, as well as for the defect-site EOMs (20) and (21) at $j = L/2$ and $j = (L/2) + 1$, respectively.

We now consider Case II: $N^* = N_0$, for which the effective boundary rates are given by $\alpha_{\text{eff}} = \alpha f(N_R)$ and $\beta_{\text{eff}} = \beta(1 - f(N_R))$, where $f(N_R) = N_R/N_0$ and $0 \leq \mu < \infty$. In this case, the EOMs (18), (20), and (21) remain invariant under the transformation (23), as for $N^* = L$. However, the boundary-site EOMs (17) and (19) are *not* invariant under the transformations (22)–(24). Under transformation (23), the densities transform as $\rho_1 \leftrightarrow 1 - \rho_L$ and $\rho_2 \leftrightarrow 1 - \rho_{L-1}$, just as in the $N^* = L$ case. However, the transformation of the function $f(N_R)$ now differs. Using the PNC, we obtain:

$$f(N_R) = \frac{N_R}{N_0} = 1 - \frac{1}{\mu L} \sum_{j=1}^L \rho_j. \quad (28)$$

Applying transformation (23) and (24) to Eq. (28) yields:

$$f(N_R) \leftrightarrow 1 - \frac{1}{(2 - \mu)} \left(1 - \frac{1}{L} \sum_{j=1}^L \rho_j \right). \quad (29)$$

Therefore, transformations (22) and (29) together imply:

$$\alpha_{\text{eff}} = \alpha f(N_R) \leftrightarrow \beta \left[1 - \frac{1}{(2 - \mu)} \left(1 - \frac{1}{L} \sum_{j=1}^L \rho_j \right) \right] \neq \beta_{\text{eff}}. \quad (30)$$

Hence, the entry-site EOM (17) does not, in general, map to the exit-site EOM (19), except when $\mu = 1$, for which the transformation $\alpha_{\text{eff}} \leftrightarrow \beta_{\text{eff}}$ holds—similar to the case $N^* = L$. Therefore, *only* for $\mu = 1$, the EOMs (17)–(21) remain invariant under the transformations (22)–(24) in the case $N^* = N_0$. At $\mu = 1$, the phase diagram corresponding to $N^* = N_0$ is identical to that of $N^* = L$. In general, there is no transformation of μ akin to the one for $N^* = L$, which can keep the dynamics of $N^* = N_0$ invariant. This shows the lack of a particle-hole symmetry in $N^* = N_0$.

DENSITY OF THE BOUNDARY SITES IN UDW PHASE

In the UDW phase, the segments T_A and T_B are in the HD and LD phases, respectively, with bulk densities

$$\rho_{LD} = \frac{q}{1+q} = 1 - \rho_{HD}, \quad (31)$$

in both cases, $N^* = L$ and $N^* = N_0$. This bulk profile is accompanied by boundary layers at the sites $j = 1$ and $j = L$ whose thickness vanishes in the thermodynamic limit. We now determine the height of these boundary layers using mean-field theory.

The time evolution of the densities at the entry and exit sites, ρ_1 and ρ_L , is governed by Eqs. (17) and (19). In the steady state, we have $\partial_t \rho_1 = \partial_t \rho_L = 0$, with $\rho_2 = \rho_{HD} = 1 - \rho_{LD}$ and $\rho_{L-1} = \rho_{LD}$ [see Eq. (31)] in the UDW phase. Solving these equations for ρ_1 and ρ_L then yields:

$$\rho_1 = \frac{\alpha_{\text{eff}}}{\alpha_{\text{eff}} + \rho_{LD}}, \quad \rho_L = \frac{\rho_{LD}}{\rho_{LD} + \beta_{\text{eff}}}. \quad (32)$$

While ρ_{LD} and ρ_{HD} are independent of the normalization constant N^* [see Eq. (31)], the effective boundary rates α_{eff} and β_{eff} generally differ between the two cases $N^* = L$ and $N^* = N_0$. To determine them, we apply particle number conservation in each case.

Case I: $N^ = L$.* Here, the effective boundary rates are $\alpha_{\text{eff}} = \alpha N_R/L$ and $\beta_{\text{eff}} = \beta(1 - N_R/L)$. The number of particles in segments T_A and T_B are $L\rho_{HD}/2$ and $L\rho_{LD}/2$, respectively. The PNC equation becomes:

$$\begin{aligned} \mu &= \frac{N_R}{L} + \frac{1}{L} \cdot \frac{L}{2}, \\ \Rightarrow \frac{N_R}{L} &= \mu - \frac{1}{2}. \end{aligned} \quad (33)$$

This gives

$$\alpha_{\text{eff}} = \alpha \left(\mu - \frac{1}{2} \right), \quad \beta_{\text{eff}} = \beta \left(\frac{3}{2} - \mu \right). \quad (34)$$

Substituting Eq. (34) into Eq. (32) yields:

$$\rho_1 = \left[1 + \frac{q}{(1+q)\alpha \left(\mu - \frac{1}{2} \right)} \right]^{-1}, \quad (35)$$

$$\rho_L = \left[1 + \frac{(1+q)\beta \left(\frac{3}{2} - \mu \right)}{q} \right]^{-1}. \quad (36)$$

Case II: $N^ = N_0$.* In this case, $\alpha_{\text{eff}} = \alpha N_R/N_0$ and $\beta_{\text{eff}} = \beta(1 - N_R/N_0)$. Applying PNC as before, we obtain:

$$\frac{N_R}{N_0} = 1 - \frac{1}{2\mu}, \quad (37)$$

which leads to:

$$\alpha_{\text{eff}} = \alpha \left(1 - \frac{1}{2\mu} \right), \quad \beta_{\text{eff}} = \frac{\beta}{2\mu}. \quad (38)$$

Substituting Eq. (38) into Eq. (32) gives:

$$\rho_1 = \left[1 + \frac{q}{(1+q)\alpha \left(1 - \frac{1}{2\mu} \right)} \right]^{-1}, \quad (39)$$

$$\rho_L = \left[1 + \frac{(1+q)\beta}{2\mu q} \right]^{-1}. \quad (40)$$

Thus, while the bulk densities in the UDW phase [Eq. (31)] are universal—depending only on the parameter q and not on other control parameters α , β , μ , or the normalization constant N^* —the boundary densities [Eqs. (35), (36), (39), and (40)] explicitly depend on all control parameters α , β , μ , q and also N^* , and are therefore nonuniversal. Furthermore, for both $N^* = L$ and $N^* = N_0$, as α and β increase while μ and q are held fixed, we observe that $\rho_1 \rightarrow 1$ and $\rho_L \rightarrow 0$, whereas the domain wall remains pinned at $x = 1/2$. See Figs. 5(a) and 5(b) for the formation of boundary layers for $N^* = L$ and $N^* = N_0$ respectively.

DELOCALIZATION OF THE DOMAIN WALLS

We here discuss in details the delocalization of domain walls for α , β falling on the curve given by Eq. (15) in the main text, which separates defect-controlled (green) and reservoir-controlled regions (yellow) in the $(\alpha-\beta)$ plane (see the phase diagrams in Fig. 2 of the main text). In the TASEP segments T_A and T_B , nonuniversal DDWs emerge in pair along the curve (15) in the $\alpha-\beta$ plane (see main text), the extent of which depends explicitly on the value of μ and q . Complete delocalization, i.e., when the DDWs span the entire TASEP segments, occurs at the point $(\tilde{\alpha}, \tilde{\beta})$ in the $\alpha-\beta$ plane given by Eq. (16) of the main text, where all phases meet [red triangle in Figs. 2(b), 2(c), and 2(e) of the main text]. Moving away from this point on both directions along the curve (15) of the main text, spatial spans of the DDWs across the segments of the TASEP lane gradually decreases and eventually vanishes at the end points marked \blacklozenge and \blacklozenge in the phase diagrams in Figs. 2(a)-2(e) of the main text. Full delocalization is seen in Fig. 3(c) ($\alpha = \beta = 0.19$, $\mu = 1$, $q = 0.1$, $N^* = L$) and Fig. 3(f) ($\alpha = 0.333$, $\beta = 0.1332$, $\mu = 0.7$, $q = 0.1$, $N^* = N_0$) of the main text. In the main text, partial delocalization for $N^* = L$ is shown in Fig. 4(a) ($\alpha = 0.154$, $\beta = 0.25$, $\mu = 1$, $q = 0.1$), Fig. 4(b) ($\alpha = 0.103$, $\beta = 0.95$, $\mu = 1$, $q = 0.1$) on one side of the point $(\tilde{\alpha}, \tilde{\beta})$, and in Fig. 4(c) ($\alpha = 0.25$, $\beta = 0.154$, $\mu = 1$, $q = 0.1$) on the other side. Clearly, as we move away from $(\tilde{\alpha}, \tilde{\beta})$ on the curve (15) in the $\alpha-\beta$ plane, the degree of

delocalization decreases, as seen in Figs. 4(a) and 4(b) of the main text. The DDWs in Figs. 4(a) and 4(c) of the main text are related by particle-hole symmetry, i.e., by the transformations (22)-(24).

We obtain the coordinates of the endpoints marked \blacklozenge and \blacklozenge of the curve (15) of the main text separating the defect- and reservoir-controlled regions in the α - β plane in the following way. Point marked \blacklozenge lies at

the junction of the LD-LD/LD-DW, LD-LD/DW-LD, and LD-DW/DW-LD phase boundaries, whereas point marked \blacklozenge is located at the intersection of the HD-HD/DW-HD, HD-HD/HD-DW, and DW-HD/HD-DW boundaries. These boundaries are obtained for both cases $N^* = L$ and $N^* = N_0$, as detailed in the main text. The coordinates of these points, obtained for each case, are listed below in Table I:

TABLE I: Coordinates of points marked \blacklozenge and \blacklozenge in the α - β plane for two representative cases

Case \ Point	\blacklozenge	\blacklozenge
I. $N^* = L$	$\left(\frac{q}{\mu(1+q) - q}, \frac{q}{1 + 2q - \mu(1+q)} \right)$	$\left(\frac{q}{\mu(1+q) - 1}, \frac{q}{2 + q - \mu(1+q)} \right)$
II. $N^* = N_0$	$\left(\frac{\mu q}{\mu(1+q) - q}, \mu \right)$	$\left(\frac{\mu q}{\mu(1+q) - 1}, \mu q \right)$

Hence, the coordinates of points \blacklozenge and \blacklozenge depend explicitly on the parameters μ and q . Since $\alpha, \beta > 0$ by definition, this imposes the following conditions presented in

Table II for the existence of points \blacklozenge and \blacklozenge in the two cases:

TABLE II: Conditions for the existence of points \blacklozenge and \blacklozenge for two representative cases

Case \ Point	\blacklozenge	\blacklozenge
I. $N^* = L$	$\frac{q}{1+q} < \mu < \frac{1+2q}{1+q}$	$\frac{1}{1+q} < \mu < \frac{2+q}{1+q}$
II. $N^* = N_0$	$\mu > \frac{q}{1+q}$	$\mu > \frac{1}{1+q}$

As illustrated in Fig. 2(a) of the main text, for $N^* = L$ and $\mu = q = 0.1$, only the LD-LD, LD-DW, and DW-LD phases are realized, leading to the appearance of their common intersection point \blacklozenge , while the HD-HD, DW-HD, and HD-DW phases are absent, and consequently, the corresponding point \blacklozenge does not appear. In Fig. 2(b) of the main text, for $N^* = L$ and $\mu = 0.7, q = 0.1$, the DW-HD and HD-DW phases are present, but the HD-HD phase remains absent. As a result, the point \blacklozenge is again not observed, whereas the point \blacklozenge persists due to the continued presence of the LD-LD, LD-DW, and DW-LD phases. In contrast, Fig. 2(c) of the main text, corresponding to $N^* = L$ and $\mu = 1, q = 0.1$, displays both intersection points \blacklozenge and \blacklozenge , as all six phases—LD-LD, LD-DW, DW-LD, HD-HD, DW-HD, and HD-DW—are simultaneously present. A similar pattern is observed

for $N^* = N_0$ in Figs. 2(d) and 2(e) of the main text, with $\mu = q = 0.1$ and $\mu = 0.7, q = 0.1$, respectively. Finally, in Fig. 2(f) of the main text, corresponding to $\mu = 1000, q = 0.1$, the phase diagram is dominated by HD-HD, HD-DW, and UDW phases, with other phases confined to very small values of α ; hence, both intersection points \blacklozenge and \blacklozenge are present but not shown. These observations from Monte Carlo simulations are in full agreement with the mean-field conditions summarized in Table II.

We now analyze the position and spatial span of DDWs occurring for points (α, β) lying on the curve (15) of the main text to determine their degree of delocalization. Consider a pair of DDWs located with mean positions at x_0 in T_A and at $(1/2 + x_0)$ in T_B . At the delocalization transition, the conditions for a DW is satisfied in

both T_A and T_B , see Refs.[16, 23, 41]. Thus the DDW envelops in T_A and T_B should be statistically identical. Following [23, 41], we use this to provide an analytical (geometric) construction of the DDW envelops in T_A and T_B . Current conservation ($J_{\text{def}} = J_{\text{res}}$) with α, β on Eq. (15) of the main text gives

$$\rho_{\text{LD}} = \frac{\alpha\beta}{\alpha + \beta} = \frac{q}{1 + q} = 1 - \rho_{\text{HD}}, \quad (41)$$

for both $N^* = L$ and $N^* = N_0$, see Eqs. (6) and (12) of the main text. We apply PNC separately for $N^* = L$ and $N^* = N_0$ to obtain the mean position of the DDW. Recall that the filling factor is defined as $\mu = N_0/L$, and for a DDW, the low-density reads $\rho_{\text{LD}} = \alpha_{\text{eff}} = 1 - \rho_{\text{HD}}$ (according to current conservation). Hence, $\rho_{\text{LD}} = \alpha N_R/L$ for $N^* = L$, and $\rho_{\text{LD}} = \alpha N_R/N_0$ for $N^* = N_0$. Denoting the particle numbers in T_A and T_B as N_A and N_B , respectively, PNC reads for $N^* = L$:

$$\begin{aligned} N_0 &= N_R + N_A + N_B, \\ \Rightarrow \mu &= \frac{\rho_{\text{LD}}}{\alpha} + \int_0^{x_0} \rho_{\text{LD}} dx + \int_{x_0}^{\frac{1}{2}} \rho_{\text{HD}} dx \\ &\quad + \int_{\frac{1}{2}+x_0}^1 \rho_{\text{LD}} dx + \int_{\frac{1}{2}}^{\frac{1}{2}+x_0} \rho_{\text{HD}} dx. \end{aligned} \quad (42)$$

Solving Eq. (42) for x_0 , we obtain

$$x_0 = \frac{1 - \mu - \rho_{\text{LD}} \left(1 - \frac{1}{\alpha}\right)}{2(1 - 2\rho_{\text{LD}})}, \quad (43)$$

where ρ_{LD} is given by Eq. (41). Similarly, for $N^* = N_0$, we get

$$x_0 = \frac{1 - \mu - \rho_{\text{LD}} \left(1 - \frac{\mu}{\alpha}\right)}{2(1 - 2\rho_{\text{LD}})}, \quad (44)$$

with ρ_{LD} again given by Eq. (41). Depending on α, β for fixed values of μ and q , the DW position, x_0 , obtained in Eqs. (43) and (44) can be greater than [see Figs. 4(a) and 4(b) of the main text], equal to [see Figs. 3(c) and 3(f) of the main text], or less than [see Fig. 4(c) of the main text] $1/4$. DDW span, Δ , is obtained from the geometric constructions of DDWs in Fig. 4 of the main text as

$$\Delta = \begin{cases} 1 - 2x_0, & \text{for } x_0 > 1/4, \\ 1/2, & \text{for } x_0 = 1/4, \\ 2x_0, & \text{for } x_0 < 1/4, \end{cases} \quad (45)$$

for both $N^* = L$ and $N^* = N_0$.

We will now compare x_0 and Δ obtained from MCS in Fig. 4 of the main text with those obtained analytically in Eqs. (43), (44), and (45) above. We consider only the case $N^* = L$ with $\mu = 1, q = 0.1$ for which the point of complete delocalization is $(\tilde{\alpha}, \tilde{\beta}) = (0.19, 0.19)$, see Eq. (16) of the main paper. In Fig. 4(a) of the main

text with $\alpha = 0.154, \beta = 0.25$, we get $x_0 = 0.32$ and $\Delta = 1 - 2x_0 = 0.36$. In Fig. 4(b) of the main text, with $\alpha = 0.103, \beta = 0.95$, we find $x_0 = 0.49$ and $\Delta = 1 - 2x_0 = 0.02$. These results indicate that the degree of delocalization of the DW decreases as one moves away from the point of complete delocalization, i.e., $(\tilde{\alpha}, \tilde{\beta})$. Finally, in Fig. 4(c) of the main text, for $\alpha = 0.25, \beta = 0.154$, we obtain $x_0 = 0.18$ and $\Delta = 2x_0 = 0.36$. All these analytical results match very well with the values of x_0 and Δ obtained by MCS.

DOMAIN WALLS IN UDW AND LD-HD PHASES

We present in this section the domain wall profiles for representative parameter sets lying in the UDW and LD-HD phases.

In the defect-dominated UDW phase, the domain wall is pinned at $x = 1/2$ irrespective of any control parameters, separating HD and LD regions appearing on segments T_A and T_B , respectively. Boundary layers of vanishing thickness in TL form on both sides of the reservoir at sites $j = 1$ and $j = L$. The bulk densities on either domains of the UDW are given by

$$\rho_{\text{LD}} = \frac{q}{1 + q} = 1 - \rho_{\text{HD}}, \quad (46)$$

indicating that both densities depend solely on the defect strength q , and are independent of α, β, μ , or the choice of the function f . The resulting domain wall is thus universal. Figs. 5(a) ($N^* = L$) and 5(b) ($N^* = N_0$) illustrate such universal domain walls for two distinct parameter sets with identical $q = 0.1$. In both cases, the wall position $x_w = 1/2$ and height given by

$$\rho_{\text{HD}} - \rho_{\text{LD}} = \frac{1 - q}{1 + q} = 0.816,$$

remain independent of α, β, μ, f , demonstrating the universal nature of UDWs vis-à-vis these parameters; see Fig. 5. Furthermore, boundary layers are observed at both ends of the TASEP lane; see Fig. 5. This is consistent with MFT predictions.

In addition to the universal domain walls observed in the UDW phase, we also find domain walls along the reservoir-controlled LD-HD phase line $\mathcal{L}(\alpha, \beta, \mu) = 0$ (see Eq. (14) in the main text) with bulk densities in the LD and HD domain appearing on the segments T_A and T_B respectively given by

$$\rho_{\text{LD}} = \frac{\alpha\beta}{\alpha + \beta} = 1 - \rho_{\text{HD}}, \quad (47)$$

These walls are likewise located at $x = 1/2$, similar to the UDWs, but their height

$$\rho_{\text{HD}} - \rho_{\text{LD}} = 1 - \frac{2\alpha\beta}{\alpha + \beta},$$

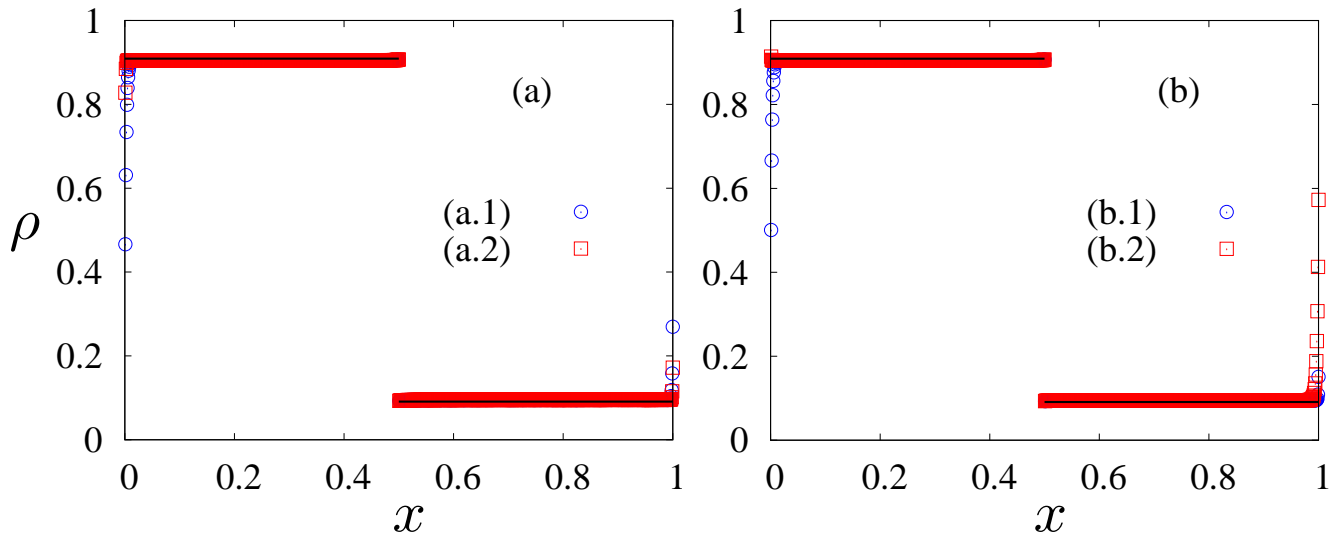


FIG. 5: Universal domain walls in the UDW phase. (a) corresponds to $N^* = L$, with parameters: (a.1) $\alpha = 0.8, \beta = 0.4, \mu = 0.7, q = 0.1$ and (a.2) $\alpha = \beta = 1, \mu = 1, q = 0.1$; while (b) corresponds to $N^* = N_0$, with parameters: (b.1) $\alpha = 0.6, \beta = 0.8, \mu = 0.7, q = 0.1$ and (b.2) $\alpha = 150, \beta = 300, \mu = 1000, q = 0.1$. The domain walls in both cases occur at the same position, $x_w = 1/2$, and have the same height $\frac{1-q}{1+q} = 0.816$, which depends only on the defect strength q , and not on α, β, μ, N^* or f . This demonstrates the universality of the UDW profile with respect to these parameters. MFT predictions (solid black line) and MCS results (colored points) match very well. The UDWs are accompanied by boundary layers at the entry- and exit-ends of TASEP.

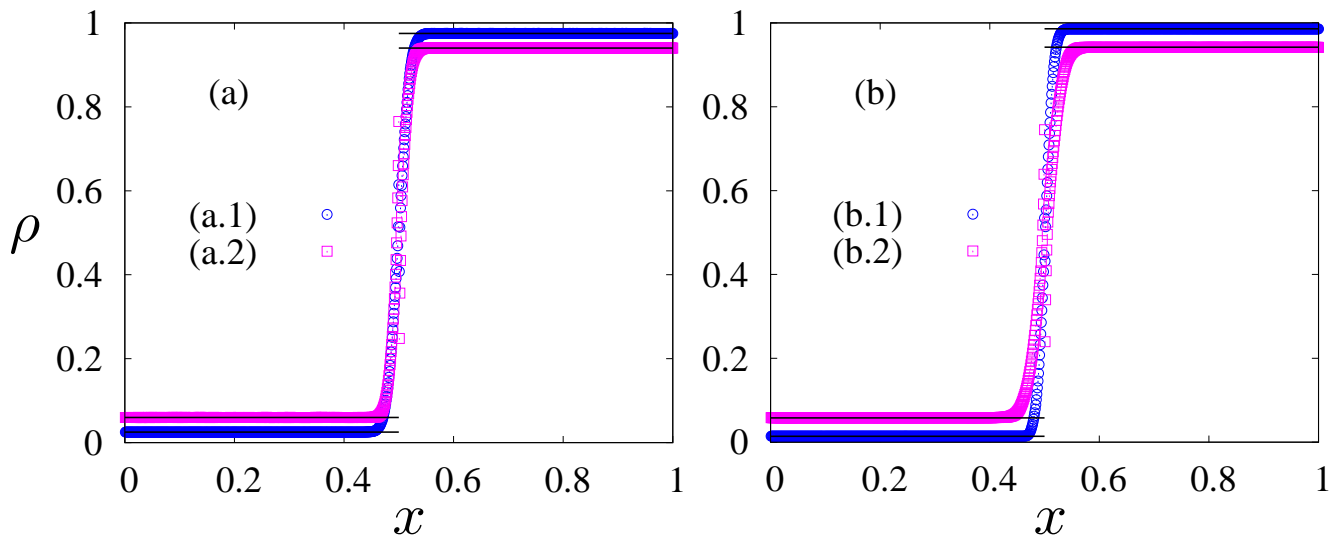


FIG. 6: Nonuniversal domain walls in the LD-HD phase. (a): $N^* = L$ with (a.1) $\alpha = \beta = 0.05, \mu = 1, q = 0.1$ and (a.2) $\alpha = 0.3, \beta = 0.075, \mu = 0.7, q = 0.1$; (b): $N^* = N_0$ with (b.1) $\alpha = 0.05, \beta = 0.02, \mu = 0.7, q = 0.1$ and (b.2) $\alpha = 0.07, \beta = 0.35, \mu = 3, q = 0.1$. In all cases, domain walls are located at $x = 1/2$, but their height, $1 - \frac{2\alpha\beta}{\alpha+\beta}$, depends on the boundary parameters α and β , reflecting their nonuniversal nature. MFT predictions (solid black lines) show excellent agreement with MCS data (colored points).

depends explicitly on the boundary parameters α and β , rendering them nonuniversal. Apart from the issue of universality, although both UDWs and nonuniversal DWs are located at $x = 1/2$, there is a fundamental distinction between the two. The HD segment of a UDW

covers T_A and the LD segment covers T_B . In contrast, a nonuniversal DW formed for α, β on the LD-HD line in the α - β plane has its LD segment covering T_A and the HD segment covering T_B . The mean-field theory predictions for the density profiles in the LD-HD phase are validated

by Monte Carlo simulation results, as shown in Figs. 6(a) for $N^* = L$ and 6(b) for $N^* = N_0$.